RESEARCH ARTICLE
doi: 10.2306/scienceasia1513-1874.2025.s018

ScienceAsia 51S (2): 2025: ID 2025s018: **1–11**

An algorithm for illuminating n non-overlapping circular discs' boundaries on the plane with application to tree stem illumination problem

Phapaengmuang Sukkasem[a], **Supanut Chaidee**[b,*], **Watit Khokthong**[c,d]

[a] Program in Applied Mathematics, Department of Mathematics, Faculty of Science, Chiang Mai University, Chiang Mai 50200 Thailand

[b] Advanced Research Center for Computational Simulation (ARCCoS), Department of Mathematics, Faculty of Science, Chiang Mai University, Chiang Mai 50200 Thailand

[c] Forest Restoration Research Unit, Department of Biology, Faculty of Science, Chiang Mai University, Chiang Mai 50200 Thailand

[d] Environmental Science Research Centre, Faculty of Science, Chiang Mai University, Chiang Mai 50200 Thailand

[*]Corresponding author, e-mail: supanut.c@cmu.ac.th

Received 1 Dec 2024, Accepted 24 Jul 2025
Available online 18 Aug 2025

ABSTRACT: Given a set of n non-overlapping circular discs on a plane, we aim to determine possible positions of points (referred to as cameras) that could fully illuminate all the circular discs' boundaries. This work presents a geometric approach for determining feasible camera positions that would provide total illumination of all circular discs. The Laguerre Delaunay triangulation, coupled with the intersection of slabs formed by the boundaries of circular discs, is employed to form the region that satisfies the given conditions. The experiment is conducted using a set of randomly positioned circular discs on a plane. This study has the potential to address the issue of illumination in forests by utilizing a terrestrial LiDAR to determine the possible number and placement of cameras that can effectively illuminate tree stems within a forest.

KEYWORDS: terrestrial laser scanner, illumination problem, slabs

MSC2020: 52C30 52C35 68U05

INTRODUCTION

In our everyday observation, as well as in mathematical views such as rooms or open areas with obstacles, we have the challenge of identifying the regions to circumvent obstructions in the visual field. From a mathematical perspective, the illumination problem is well established in discrete and computational geometry [1]. The main issue of illumination problems [2] is to find the least number of lighting points to obtain the highest illumination efficiency and to place the lighting source so that it can illuminate the area or object [3]. There are widely known problems in the illumination problem, such as the Art Gallery problem [3–5], the Guarding problem [6, 7], and the floodlight illumination problem [8, 9]. In various conditions for illumination, the lighting source that is positioned can be projected to test the efficiency.

A practical example of the challenge of illumination is the use of LiDAR (Light Detection and Ranging) sensors to illuminate forest structures for environmental research [10]. Forest practitioners have utilized the LiDAR [11] and camera sensors, which employ laser motion capture technology, to illuminate the structure of forests. Focusing on the LiDAR, regarded as a light source capable of emitting illumination in all directions, the challenge lies in identifying the optimal position for the LiDAR laser scanner to maximize the capture of forest structural information. Recent studies focused on the suggestion of the use of terrestrial laser scanner (TLS), which is a highly accurate remote sensing technology that captures the three-dimensional geometry of objects by emitting laser pulses from a ground-based device, generating a dense point cloud that represents the scanned environment in detail, with forest. A study in Abegg et al [12], investigated the impact of different patterns of placement of scanners on visibility within forest plots when using terrestrial laser scanning. By simulating various scanning patterns and positions, the study demonstrated that the arrangement and number of scanning locations significantly influence mean visibility. Another study by Wilkes et al [13] discussed the use of TLS to capture detailed forest structure data on extensive plots. The study recommended a systematic grid pattern for the scan position locations, highlighting the effectiveness of a 10 m $\times$ 10 m grid in achieving uniform point distribution.

The challenge of non-detection in single scan TLS of forests is addressed in a study from 2019 [14], which can miss some tree stems or other vegetative parts that are obscured by others. It introduced a new estimator in terms of marked point pattern of trees that compensates for these non-detection results,

by considering different detection rules, which model partial or nearly full or visibility of a standing tree. The study in 2020 [15] proposed an Iterative-Mode Scan Design for TLS in forests to minimize occlusion effects and improve accurate tree attribute estimation. The method evaluates the potential location for the scan using a PoTo index and the cumulative degree of ring closure (CDRC) to enhance the completeness of the scan, particularly in dense stands.

Although the previously mentioned literature has suggested basic strategies for gathering tree-root information from TLS LiDAR, the specific procedure for determining the optimal placement of the active sensor remains improperly explored. To model this problem mathematically, we can represent the cross-section of the trees as a set of circular discs, with the TLS LiDAR serving as the emission light source. We aim to identify the optimal positions for TLS LiDAR to effectively illuminate a specified set of circular discs that can represent tree stems and to minimize the number of sources while maximizing the illuminated area.

The study of Tóth [16] explores the illumination of convex discs and explains how a set of n circular discs can be illuminated by $2n$ points. Then there is more study of scenarios where circular discs overlap or are centered on a line. The concept of a generalized Voronoi diagram is used to describe how vertices can illuminate the corresponding arcs of a circular disc. Theorems are presented to establish upper bounds for the required number of lighting points, affirming the sufficiency of $2n$ points, and suggesting $\max(2n, 4n-7)$ points as necessary for non-overlapping open convex discs. Those propose more results and combinatorial aspects in the art gallery problem in point guard and edge guard [3, 17].

In this paper, we present a geometrical approach to ascertain the locations of light sources required for the total illumination of a collection of circular discs, guaranteeing that each circular disc is entirely illuminated by the sources. A slab characterized by a region bounded by parallel lines formed by two adjacent circular discs will be investigated to establish a feasible region for the placement of light sources. We prove the geometrical properties of intersecting slabs, then utilize these areas as potential locations for source placement, and propose an algorithm that addresses the problem. Subsequently, we conduct experiments to determine the optimal scenario using ideally generated data comprising both identical and varied circular discs. We also use artificial trees and utilize LiDAR to illuminate these trees, so obtaining the illuminated region serves as validation from the computations to quantify the accuracy from the ideally generated data.

This paper is organized as follows. The Introduction includes a related review on the research topic. In the second section (Preliminaries), we provide a basic background in computational geometry, which we have used in this study. In addition, we formulate the problem to tackle in this part. The geometrical properties of the illuminating region will be investigated in Section 3 (Geometrical properties of the illuminating region), including an algorithm to locate the illuminating location. In Section 4 (Experiment), we perform experiments to verify the proposed algorithm. We finally conclude our study in the last section of this paper (Concluding remark).

PRELIMINARIES

Background in computational geometry

The *convex hull* [18] of a set S, denoted $CH(S)$, is the smallest convex set that contains S. It is the intersection of all convex sets that contain S, i.e., for any $\alpha \in \Lambda$ and C_α a convex set covering S, $CH(S) = \bigcap_{\alpha\in\Lambda} C_\alpha$. There are several algorithms to compute the convex hull from a set of finite points on the plane, such as divide and conquer. The time complexity of the convex hull algorithm is known to be $O(n \log n)$.

A point p on a convex hull of a convex set S is said to be *visible* [19] to an illuminating point q if and only if the line segment connecting p to q does not intersect the interior of S. A segment P of convex hull of S is said to be *illuminated* by the illuminating point q if all points in P are visible to q. For a circular disc, a circular arc of the disc acts as an illuminated segment of a convex hull. Fig. S2(a) illustrates the visibility of points on a circular arc.

The *illumination problem* is a classic problem to find the location of the light source s that an object O is visible to s. We call s an illuminating point and O is illuminated by s. It is remarked that the boundary of a convex set in the plane can always be illuminated by using three light points [2].

One of the most used diagrams in computational geometry is the Voronoi diagram, as compiled in the book [20]. Let $P = \{p_i, \ldots, p_n\}$ be a set of points on a plane called a set of generator points, and let $d_E(p, p_i)$ denote the Euclidean distance between the points p and p_i on the plane. The Voronoi region $V(p_i)$ of a site p_i in P is

$$V(p_i) = \big\{p \in \mathbb{R}^2 \mid d_E(p, p_i) \leqslant d_E(p, p_j) \quad \text{for all } j = 1, \ldots, n \text{ and } j \neq i\big\},$$

such that the Voronoi diagram [18] of a generator set P is the Voronoi region written as $Vor(P) = \{V(p_i), \ldots, V(p_n)\}$. The *ordinary Voronoi diagram* corresponds to the Voronoi edges and Voronoi vertices that divide the plane into regions with the Euclidean distance. The cells of the partitioning of a plane are called Voronoi polygons. The *Delaunay triangulation* [18] is generated by the line segments between p_i and p_j for all i and j that the boundaries of $V(p_i)$ and $V(p_j)$ share a common edge.

Based on Tóth [16], which discusses the use of the vertex of the Laguerre Voronoi diagram as the placement of light points, the definition of the Laguerre Voronoi diagram and the Laguerre Delaunay triangulation are necessary to declare, which is the duality of each other. Assume a set of n circular discs in the plane $G = \{C_i, \ldots, C_n\}$ is given. Let r_i and $p_i = (x_i, y_i)$ be the radius and the center of the circular disc C_i, respectively. For a disc C_i and point $p = (x, y)$ in the plane, we define the Larguerre distance (or power distance), which is the distance between a circle C_i and point p by

$$d_L(p, C_i) = d(p, p_i)^2 - r_i^2.$$

Let us define

$$V_L(G, C_i) = \left\{ p \in \mathbb{R}^2 | d_L(p, C_i) \leqslant d_L(p, C_j) \text{ for all } i \neq j \right\}.$$

The plane is partitioned into $V_L(G, C_i), \ldots, V_L(G, C_n)$ and their boundaries. The partition is called the *Laguerre Voronoi diagram* [21, 22] or the power diagram.

For a given set G of n circular discs, the *Laguerre Delaunay diagram* [23] is generated by the following procedure. Remark that a line segment between p_i and p_j is drawn if and only if the boundaries of $V_L(G, C_i)$ and $V_L(G, C_j)$ share a common edge. For circular disc C_i, we define C_i^* as the 3D point mapped by $(x_i, y_i) \mapsto x_i^2 + y_i^2 - r_i^2$; i.e., defined by $(x_i, y_i, x_i^2 + y_i^2 - r_i^2)$ for $i = 1, \ldots, n$, and define $G^* = \left\{ C_i^*, \ldots, C_n^* \right\}$. We then construct the three-dimensional convex hull $CH(G^*)$ and project its lower hull onto the two-dimensional xy-plane to obtain the Laguerre Delaunay diagram.

In this study, we focus on considering regions induced by tangent lines. In general, a *slab* is the region bounded by two parallel lines l_i and l_j. In our context, the slab will be specifically defined soon.

Problem formulation

From the real-world scenarios, we suppose to have a forest with n trees. To simplify our study, we mathematically assume that trees are circular cylinders, and we are going to project the cross section of the forest into a set of n circular discs in a two-dimensional space. The problem of three-dimensional forest scanning can be addressed with the illumination problem of positioning the illuminating point that covers most of the boundaries of the n circular discs, given the LiDAR and the camera sensor as the illuminating point to illuminate the boundaries of the forest as a set of n circular discs. Our objective is to construct a deterministic geometrical algorithm to find a set of appropriate regions to position the illuminating point, the region of visibility are called feasible region constructed by intersection of slab. The definition and properties of both regions will be presented in the next section.

GEOMETRICAL PROPERTIES OF ILLUMINATING REGION

Properties of slabs

From the previous section, we are going to represent the forest as a set of circular discs and the LiDAR and camera sensors as illuminating points. Therefore, we analyze the properties of the half-plane constructed by a tangent line corresponding to a point on the circumference of the circular disc to discover the properties of an illuminating point.

Lemma 1 *Let C be a circular disc, p be a point on the circular disc C, and l_p be the tangent line to C at p. If the illuminating point q is on the side of the half-plane corresponding to l_p that does not contain C, then p is always illuminated by q.*

Proof: Let l_p be a tangent line to the circular disc C at the point p. This line defines two half-planes: one that contains the entire interior of C, and the other that contains only the point p, since p is the point of tangency. Let q be a point lying in the half-plane that does not contain the interior of C. We aim to show that the segment $\overline{pq}$ does not intersect the interior of C. Since p is the only point in C that lies in l_p, and the whole interior of C lies strictly on the opposite side of the half-plane containing q, then $\overline{pq}$ cannot intersect the interior of C. Therefore, the point p on C is always illuminated by a point q that lies in the half-plane which does not contain the interior of C. The illustration of l_p to a circular disc C is shown in Fig. S1. □

From Lemma 1, we extend the idea to two circular discs with an illuminating point. We construct two parallel tangent lines on each circular disc that correspond to the intersection point between their circumference and line segment from center of both circular discs. We define a slab as the region of intersection of two half-planes that do not contain any circular discs from parallel tangent lines. A slab will be a region for illuminating point location, by the following definition.

Definition 1 Let C_i and C_j be two non-overlapping circular discs, and let $\overline{c_i c_j}$ be the segment connecting their centers c_i and c_j. For points $p_{i,j}$ and $p_{j,i}$ which are the intersections of $\overline{c_i c_j}$ with the boundaries of C_i and C_j, respectively, and the parallel tangent lines $l_{i,j}$ and $l_{j,i}$ at $p_{i,j}$ and $p_{j,i}$corresponding to discs C_i and C_j, the region $S_{i,j}$ bounded by the pair of lines $l_{i,j}$ and $l_{j,i}$ is called a slab.

From the definition of a slab, we define the intersection points $p_{i,j}$ and $p_{j,i}$ as radial tangent points, corresponding to the circular discs C_i and C_j, respectively. The tangent lines $l_{i,j}$ and $l_{j,i}$ corresponding to both circular discs are defined in the same way. We also observe that both slab boundaries are always perpendicular to the segment connecting the centers

of the two corresponding circular discs, because of the tangency properties of the circular discs. Remark that the slab is unique up to the given size of circular discs and the distance between two circular discs. Therefore, we would verify the visible property of an illuminating point in a slab by the following lemma.

Lemma 2 *Any point on the slab always illuminates two intersection points corresponding to the boundaries of the slab.*

Proof: Let $S_{i,j}$ be the slab bounded by a pair of parallel lines $l_{i,j}$ and $l_{j,i}$, formed by circular discs C_i and C_j at their respective radial tangent points $p_{i,j}$ and $p_{j,i}$, and assume a point $q \in S_{i,j}$. We note that the slab $S_{i,j}$ is defined by the intersection of two half-planes R_i and R_j, that is, R_i is the half-plane defined by $l_{i,j}$ that does not contain the interior of C_i and R_j similarly with respect to $l_{j,i}$ and C_j. Since $q \in S = R_i \cap R_j$, the illuminating point $q \in S$ lies in both half-planes R_i and R_j. By Lemma 1, we conclude that q always illuminates $p_{i,j}$ and $p_{j,i}$. Fig. S2(b) shows an example of an illuminating point q in a slab $S_{i,j}$ which illuminates two circles C_i and C_j. □

For a collection of n circular discs, we consider neighboring circular discs using Laguerre Delaunay triangulation of those circular discs. Hence, for any nondegenerate triangulation, we construct a slab of each two circular discs from three circular discs corresponding to a triangle in the triangulation.

In fact, any convex body uses at least three illuminating points to illuminate all its boundaries [2], and half of the convex body cannot be illuminated by one illuminating point.

Intersection of slabs

In previous section, we remarked that the slab is a region between parallel lines that is used to pose the illuminating point of two circular discs. In this section, we are going to observe the intersection of slabs, which will lead to a feasible region of illuminating point position, and explore the geometric shape and properties of feasible region constructed by the intersection of three slabs generated by three circular disc.

Remark that two groups of lines that compose the slabs have different slopes. Then we observe that the region constructed by the intersection of two slabs is a parallelogram.

Definition 2 Let C_i, C_j and C_k be three non-overlapping circular discs. The region that is the intersection of three slabs constructed by these three circular discs is called *feasible region*.

Lemma 3 *The feasible region of three non-overlapping circular discs is a convex polygon.*

Proof: Given three non-overlapping circular discs C_i, C_j, and C_k, we can construct three slabs $S_{i,k}, S_{j,k}$ and $S_{i,k}$, which correspond to each pair of circular discs. Since each pair of slabs generates a parallelogram, we have three parallelograms $P_{i,k}, P_{j,k}$ and $P_{i,k}$ from the intersection of every pair of three slabs. The parallelogram is a convex polygon that is the boundary of a convex set. In fact, since the intersection of convex sets is convex, the intersection of parallelograms $P_{i,k}$, $P_{j,k}$ and $P_{i,k}$ constructs a convex region. Thus, the feasible region is a convex polygon. □

Fig. S3 shows an example of how to generate the feasible region from the slabs of each of two circles. We apply the idea of radical tangent points on two circular discs to three circular discs that can construct circular arcs on each circular disc that have these radical tangent points as their end point. We claim that this arc is the part of the boundary of the circular disc that must be illuminated by an illuminating point within its corresponding feasible region, as defined below. The illustration of the objective arcs is included with the feasible region, as shown in Fig. 1.

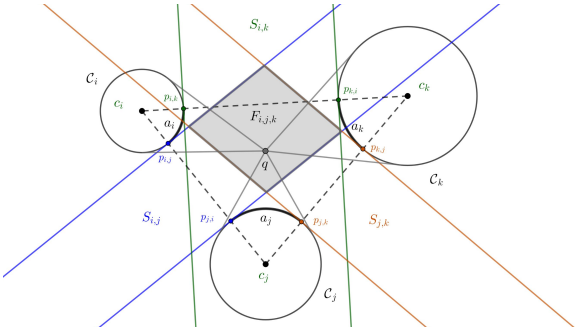

Fig. 1 A feasible region $F_{i,j,k}$ is constructed by the intersection of the slabs $S_{i,j}$, $S_{i,k}$, and $S_{j,k}$ with objective arcs a_i, a_j, and a_k, where any illuminating point $q \in F_{i,j,k}$ illuminates all three objective arcs.

Definition 3 For any three non-overlapping circular discs, circular arcs that have tangent points as endpoints and arc length that are less than half of the boundary size are called *objective arcs*.

Theorem 1 *Any point in a feasible region of three non-overlapping circular discs always illuminates all objective arcs.*

Proof: Given three non-overlapping circular discs, for each triangle of these circular discs (regarded as the triangle of Laguerre Delaunay triangulation), there are 6 intersection points between triangle edges and circular disc boundaries, which are two on each circular disc. Any two points on each circular disc form two circular arcs, which are objective arc and non-objective arc. From Lemma 2, the illuminating point can illuminate two radical tangent points on different circular discs at the same time when it lies on the slab. Since

the feasible region is the intersection of three slabs, any point in the feasible region always illuminates all points between two end points of the objective arc on each circular disc. Thus, the point on feasible region always illuminates all three objective arcs. □

From Theorem 1, the objective arcs are defined as the regions obtained from the construction of the feasible region of three circular discs. If the illuminating point lies within the feasible region, we can ensure that all objective arcs of the circular discs are illuminated by the illuminating point.

Shapes of feasible region

We consider the possible shape of a feasible region with respect to the set of circular discs by the following theorem.

Theorem 2 *The possible shape of the feasible region ranges from 4-gon to 6-gon.*

Proof: We first prove that the feasible region is not a triangle. Assume that T is a triangular feasible region with corresponding triangle $T_\triangle$ in the Laguerre Delaunay triangulation, i.e. it corresponds to the circular discs C_i, C_j and C_k, then we consider the intersection points between the boundaries of C_i, C_j, C_k and $T_\triangle$ that generate slabs $S_{i,j}$, $S_{i,k}$ and $S_{j,k}$ of each pair of circular discs.

Since the intersection of two feasible regions forms a parallelogram, the third slab in a triangular feasible region must contain at least one vertex of this parallelogram—either by crossing the edges adjacent to that vertex or by passing through at least one of its adjacent vertices.

From the construction of the feasible region, each circular disc C_i must be adjacent to a pair of tangent lines $l_{i,j}$ and $l_{i,k}$ from two different slabs. We observe that there are a total of eight possible combinations of six parallel lines: six of these correspond to triangular feasible regions that include a vertex formed by the intersection of a pair of tangent lines to a circular disc, while the remaining two correspond to triangular feasible regions that do not include such an intersection point as a vertex. Fig. S4 illustrates all eight possible cases of triangular feasible regions.

From all the mentioned types of triangular feasible region with their combination, we observe that there are two cases in constructing circular discs through the triangular feasible regions. These two case will lead to the contradiction to definition of slab and feasible region, as follows.

For the first case, we begin with constructing the first circular disc C_i with radius r centered at any pair of tangent lines. Then, we construct perpendicular lines $l^\perp_{i,j}$ and $l^\perp_{i,k}$ to the tangent lines $l_{i,j}$ and $l_{i,k}$ at the corresponding radial tangent points $p_{i,j}$ and $p_{i,k}$, respectively. For each of the remaining pairs of tangent lines, we draw angle bisectors, b_j between $l_{j,i}$ and $l_{j,k}$, and b_k between $l_{k,i}$ and $l_{k,j}$. The intersection of $l^\perp_{i,j}$ and b_j defines the center c_j of the circular disc C_j, while the intersection of $l^\perp_{i,k}$ and b_k defines the center c_k of the circular disc C_k. Connecting these centers with a segment $\overline{c_j c_k}$, we observe that this segment is not perpendicular to the slab $S_{j,k}$. This contradicts the definition of a slab, which requires that the segment connecting the centers of the two circular discs be perpendicular to both corresponding slab boundaries, as example shown in Fig. 2(a).

The second case is similarly considered as the first case. We construct the circular disc C_i with center c_i, the perpendicular lines $l^\perp_{i,j}$ and $l^\perp_{i,k}$ to the tangent lines $l_{i,j}$ and $l_{i,k}$ at the radial tangent points, and the angle bisectors b_j and b_k between the corresponding pairs of tangent lines. The center c_j is then obtained as the intersection of $l^\perp_{i,j}$ and b_j, and c_k as the intersection of $l^\perp_{i,k}$ and b_k. However, this construction results in one of the circular discs—either C_j or C_k—overlapping with another circular disc, which contradicts the hypothesis that all three circular discs are non-overlapping, as example shown in Fig. 2(b).

Secondly, it is possible to be a parallelogram (4-gon) in the case that the first two slabs intersect to be a parallelogram, and the parallel lines of the third slab concurrent the intersected points, or cover the existing parallelogram.

We can finally ensure that the maximum vertices number of feasible regions is 6, if the region of the slab covers any two non-adjacent vertices of two slab intersections, which is a parallelogram, then the slab will intersect all four edges of a parallelogram given four maximum intersection point. These four intersection points and two nonadjacent vertices of a parallelogram are vertices of the feasible region, which is 6 vertices.

We mention that we do not focus on the non-degeneracy case of triangulation, since the case gives the result of the slab that lies inside another slab. □

From our observation, if we consider a Voronoi diagram of a set of non-overlapping circular discs of the same radius, then the edges of the Voronoi diagram are the middle lines of slabs. Also, the vertices of Voronoi diagram are always in a feasible region. The examples of 4-gon, 5-gon and 6-gon of the feasible region are shown in Fig. 3.

Algorithm to illuminate circular discs

In construction of feasible regions on a set of circular discs, there is the possibility that feasible regions can overlap each other. Since the feasible region is always a convex polygon, the intersection of feasible region still be a convex polygon. Therefore, we come up with some corollary that supports our algorithm in a further section of the study.

Corollary 1 *Any point on the intersection of overlapping feasible regions illuminates all objective arcs of*

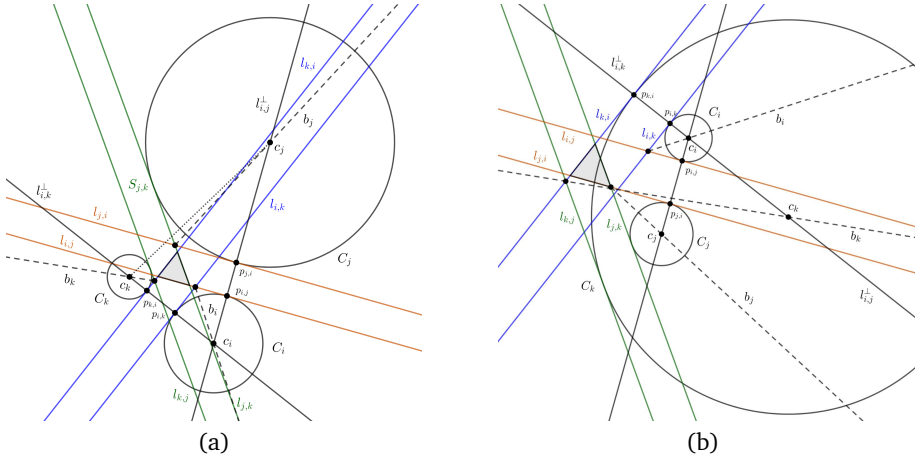

Fig. 2 (a) Example of a triangular feasible region in the first case, where the segment $\overline{c_j c_k}$ is not perpendicular to the slab $S_{j,k}$. (b) Example of a triangular feasible region in the second case, which results in overlapping circular discs.

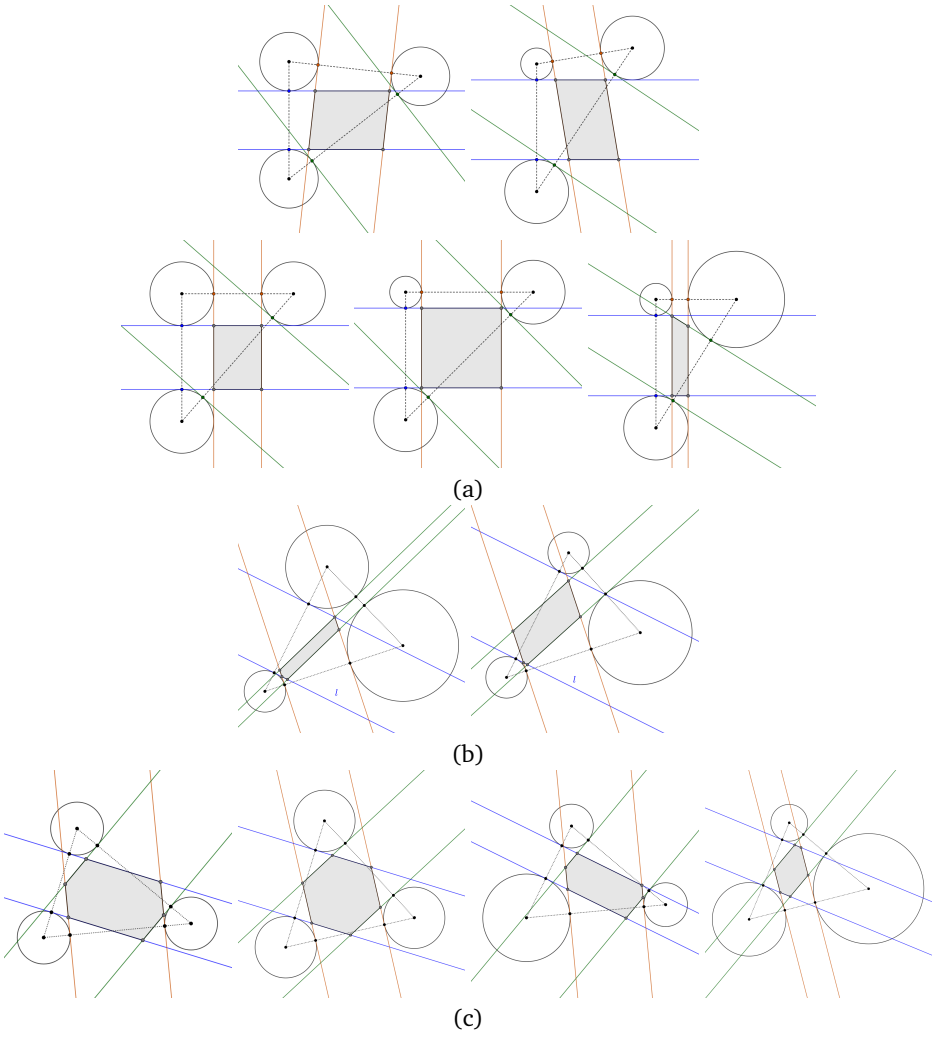

Fig. 3 Examples of feasible regions with the shape of (a) quadrilateral, (b) pentagon and (c) hexagon.

overlapping feasible regions.

Proof: From Theorem 1, any point on the feasible region will always illuminate their objective arcs. Therefore, intersection of overlapping feasible regions gives smaller regions that contain all points that still illuminate to their objective arcs. □

In our algorithm, we are going to use the fact of visibility on overlapping feasible regions to return a smaller number of a position set of illuminating points within the convex hull of a set of circular discs, which is called a curvilinear convex hull. Since any convex body can be illuminated by three illuminating points, in future work we aim to study the positioning of these three illuminating points outside the curvilinear convex hull of a set of circular discs. Therefore, in this study, we focus on positioning the illuminating point only inside the curvilinear. The main algorithm to positioning a set of illumination points is presented in Algorithm 1.

The complexity analysis of the algorithm involves several steps with varying computational costs. The construction of the Laguerre Delaunay triangulation with n points has a complexity of $O(n \log n)$ [22]. The construction of intersection points between triangles and circular arc boundaries takes $O(n)$. The construction of slabs tangent to all intersection points requires constant time, $O(1)$, since the operation involves a fixed number of tangent lines. Determining feasible regions as the intersection of six half-planes has a complexity of $O(n)$, since the number of half-planes is fixed in each triangle. Lastly, constructing the set of neighboring triangles using a search algorithm also requires $O(n)$ as it involves a search through the triangles. The most computationally expensive operation in this process is the construction of the Laguerre Delaunay triangulation $O(n \log n)$, making the overall complexity of the process $O(n \log n)$.

Algorithm 1 Feasible region computation

Require: A set $\mathscr{C}$ of n circular discs with center $C(x, y)$ and a radius r.
Ensure: A set of feasible regions Q and a set of centroid R.

Construct Laguerre Delaunay triangulation through 3D convex hull. Define C^* as a set of triangles in Delaunay triangulation, i.e. $C^* = \{\triangle_1, \ldots, \triangle_m\}$.
Construct a set of radical tangent points I between each edge of $\triangle_i \in C^*$ and boundaries of circular discs.
Construct a set of tangent lines L of $\triangle_i \in C^*$ from the radical tangent points to circular discs.
Construct a set of feasible region $F = \{F_1, \ldots, F_m\}$ of $\triangle_i \in C^*$ by half-plane intersection.
Set $Q, R = \varnothing$
while $F \neq \varnothing$ **do**
    $P = \varnothing$
    for $i = 1$ to m **do**
        if $\triangle_i$ is adjacent to $\triangle_j$ for some j **then**
            $J = F_i \cap F_j$, where
            if $J \neq \varnothing$ **then**
                $P_i \in P$
            end if
        end if
        Sort P in descending order based on $|P_i|$. ▷ If two sets P_i and P_j (with $i < j$) have the same members, then P_i should be placed before P_j.
        Define J^* as the intersection of all feasible region in P_1 and append $J^* \in Q$.
        $F := F - F_k$ for all $F_k \in P_1$.
    end for
end while
for $i = 1$ to $|Q|$ **do**
    Compute the centroid V of J_i and store $V \in R$
end for
Print Q and R.

EXPERIMENT

Setting of experiment

We applied our algorithm to the practical situation by generating position data at or close to the points of the grid. Also, we vary the different diameters of the circular discs, and then calculate the feasible region through our procedure. Each tree will be represented as a cylindrical object, specifically the PVC pipe (15.24 cm) and the paper tube (7.62 cm), and will be placed at points in the grid or at a random position inside a circular disc with a radius half the size of the grid around the point in the grid (Table 1). Fig. 4(a) shows the location of PVC pipes and paper tubes in experiment no. 1 to 5.

Our algorithm will then be used to determine camera location regions within a given forest. The centroid of feasible regions from the output will be used to position cameras to illuminate our practical situation experiments. The study will include five experiments with specific settings described in Table 1. The feasible regions from the computation using Algorithm 1 with respect to locations of pipes (circles) are shown in Fig. 4(b).

Experimental results and discussion

The TLS method is used in real-world experiment number 1 to 5, employing a LiDAR laser scanner to collect 3D point cloud data for each generated forest dataset.

We consider two types of experimental results: multiple and single scanning positions. Both results include the number of detected trees from the TLS scans and show the average illuminated boundaries of a set of circular discs, expressed as a percentage, for both the experimental and theoretical averages. The

Table 1 The setting of each experiment, including numbers of materials used for tree representation and the position of the tree center.

Experiment no.	Material of trees representation with the diameters	Number of trees	Position of trees center	Type of scanning position
1	PVC pipes (15.24 cm)	12	On grid	Single scan and multiple scans
2	PVC pipes (15.24 cm)	12	Random position around grid point	Single scan and multiple scans
3	PVC pipes (15.24 cm) Paper tubes (7.62 cm)	6 6	On grid	Multiple scans
4	PVC pipes (15.24 cm) Paper tubes (7.62 cm)	6 6	Random position around grid point	Multiple scans
5	PVC pipes (15.24 cm) Paper tubes (7.62 cm)	6 6	Random position around grid point	Multiple scans

Table 2 Results from the TLS scannings and the theoretical generated the forest structure in each experiments.

Experiment no.	No. of detected tree	Experimental average of illuminated boundaries (% ± SD)	Theoretical average of illuminated boundaries (% ± SD)
1	12	77.26 ± 13.21	77.83 ± 12.16
2	12	72.51 ± 14.92	73.42 ± 14.01
3	7	78.37 ± 11.41	82.05 ± 13.31
4	11	71.28 ± 13.82	72.66 ± 14.77
5	7	77.18 ± 14.61	81.47 ± 15.30

single scanning position results are further divided by each individual scanning point for Experiments 1 and 2, since both experiments detected all 12 trees in the multiple scanning position results.

The experimental average uses the 3DFIN plugin on CloudCompare, a specified software for illustrating and managing the 3D point clound data, to detect tree diameters and calculate the illuminated boundary of each detected tree as a percentage. The theoretical average involves plotting the generated datasets and illuminating points obtained by an algorithm in GeoGebra and using its geometric tools to construct illuminated boundaries as geometric objects. These objects are then used to extract values and compute their corresponding percentages. The percentage of illuminated boundaries was determined with the standard deviation (SD) in Table 2 and Table 3.

Experimental discussion

Compatibility between TLS scanning and the region derived from the proposed methods for the detection of tree stems at breast height (DBH), as a cylindrical object, can arise when the positions of the tree centers are on the grid. This is demonstrated by the average illuminated boundaries, which reach 78.37% and 82.05% for experiment 3 in the experimental and theoretical result, respectively. However, the small represented trees (diameter 15.24 cm) were only 58.33% detectable from multiple scans.

From single scan experiments number 1 and 2, we derived the lower illuminated boundaries from about

Table 3 Result of experiment number 1 and experiment number 2 in the single scan.

Experiment no.	Scan no.	No. of detected tree	Experimental average of illuminated boundaries (% ± SD)	Theoretical average of illuminated boundaries (% ± SD)
1	1	11	47.60 ± 2.70	48.82 ± 0.65
	2	10	49.10 ± 1.67	48.68 ± 0.57
	3	11	47.54 ± 3.13	48.82 ± 0.65
	4	11	47.98 ± 2.72	48.82 ± 0.65
	5	10	49.44 ± 1.38	48.68 ± 0.57
	6	11	47.98 ± 2.77	48.82 ± 0.65
2	1	11	47.73 ± 2.93	48.91 ± 0.58
	2	10	49.17 ± 2.17	48.64 ± 0.77
	3	11	47.92 ± 2.64	48.86 ± 0.64
	4	11	47.16 ± 3.05	48.81 ± 0.55
	5	11	46.72 ± 3.79	48.43 ± 1.49
	6	12	47.16 ± 2.45	48.72 ± 1.03

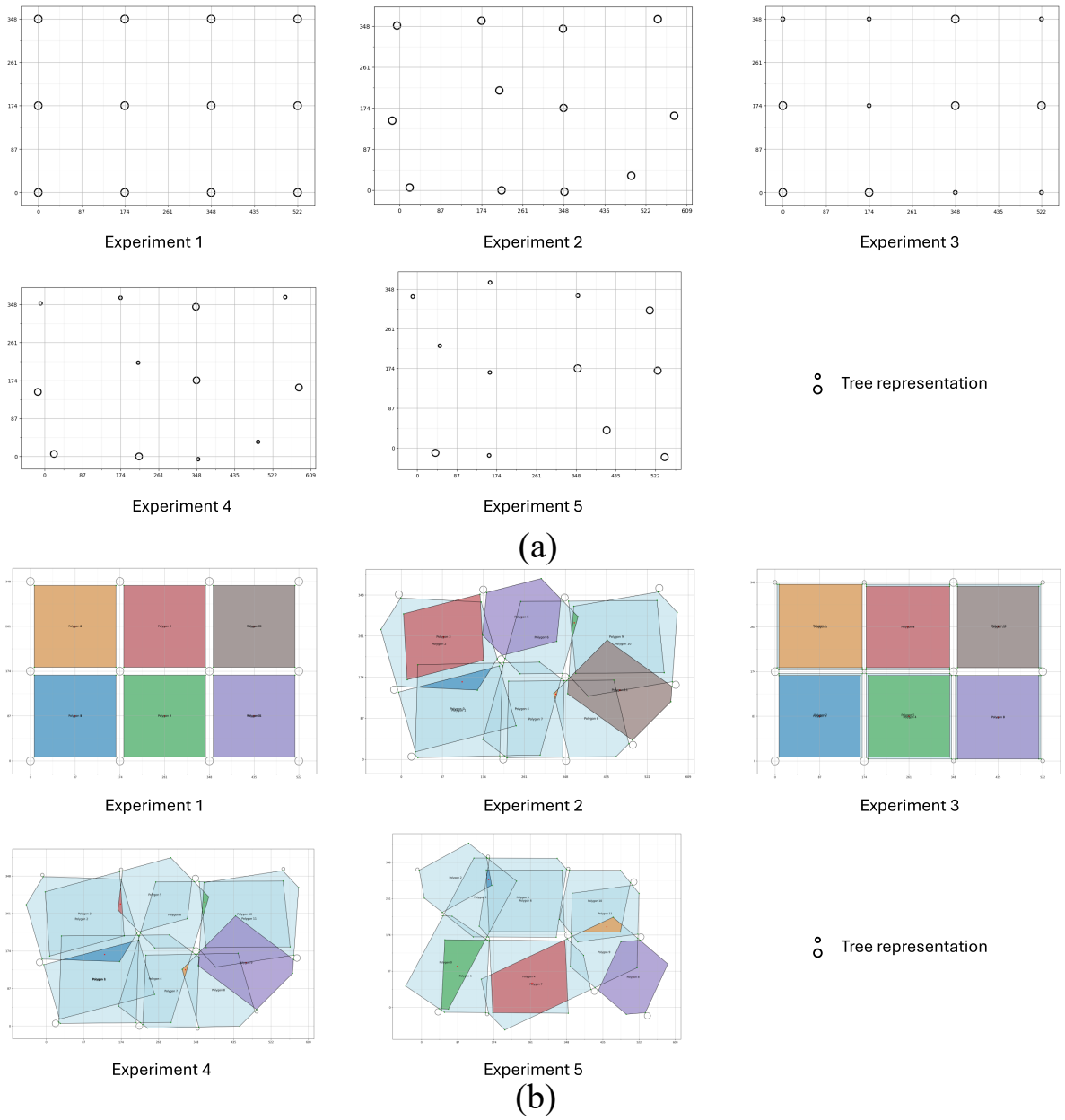

Fig. 4 (a) Position of trees in ideally generated forest of all experiments and (b) result of a set of feasible regions of ideally generated forest in each experiments.

47% to 49% that showed the proper accuracy ranges, less than maximum 50%, since one illuminating point cannot illuminate half of the boundary of the convex body [2], for tree stem detection. In addition, scan number 6 in experiment number 2 gave the 100% detected trees from a single scan (Table 3 and Fig. 5).

CONCLUDING REMARKS

We proposed a geometrical algorithm to find a set of feasible regions to position the illuminating point given as LiDAR and camera sensors to illuminate a set of circular discs given as a set of tree stems from the cross section. The algorithm uses geometric methods such as the Laguerre Delaunay triangulation and the slab to specify feasible regions for positioning the illuminating point and studying their shape. Also, we define an objective arc, which is constructed through the triangulation edges and circular disc boundaries, to be the least arc of a circular disc boundary illuminated by an illuminating point. From these geometrical objects, we come up with some theory to support the algorithm.

This study applied the algorithm to five experi-

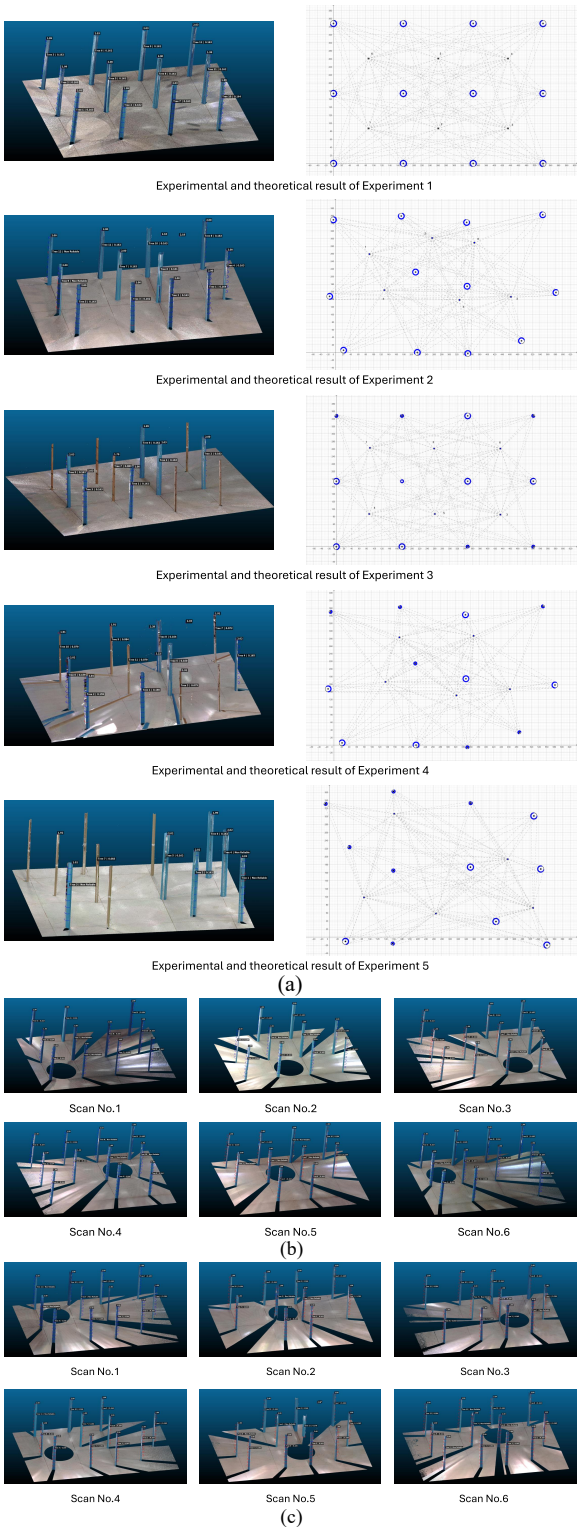

Fig. 5 (a) Comparing the experimental and theoretical results of all experiments, the full and partial blue cross-sectional circular discs represent the illuminated bounaries of trees, (b) single scans from experiment number 1, and (c) single scans from experiment number 2.

ments with practical situations by generating position data on the grid and close to the grid point and varying the different diameters of circular discs as tree stems in Table 1. Moreover, we provide two different results of the scanning position, which are multiple scan and single scan. Both different scanning positions give compatible results between TLS scanning and the region derived from the proposed methods for tree stem detection at DBH in Table 2 and Table 3. The result on average of illuminated boundaries in the percentage of a single scanning position gives proper accuracy ranges for tree stem detection.

For future work, we plan to prove mathematical methods to minimize the number of scans in tree stem illumination problems both inside and outside the curvilinear of a set of circular discs. Also, we tend to find possible shapes of the feasible region to give patterns of triangulation alignment for positioning the illuminating point in practical situations. Furthermore, we aim to improve the geometrical algorithm to perform the experiment with a real forest.

Appendix A. Supplementary data

Supplementary data associated with this article can be found at https://dx.doi.org/10.2306/scienceasia1513-1874.2025.s018.

Acknowledgements: The first author would like to thank the master's degree friends from the Department of Mathematics, Faculty of Science, Chiang Mai University, especially Asama Jampeepan, for great discussion while working on this paper. The discussions were done through Geometry Boot Camp 2023–2024, especially Nitipon Moonwichit and Nattawut Phetmak. The first author is supported by the Teaching Assistant and Research Assistant Scholarship for the Academic Year 2023–2024 from Chiang Mai University. This research is partially supported by Chiang Mai University and the experiment in this research is supported by FORRU's Small Grant Support for Student Projects. We finally thank the reviewer for the careful and constructive comments to improve the manuscript.

REFERENCES

1. Honsberger R (1976) *Mathematical Gems II (Dolciani Mathematical Expositions, No. 2)*, Mathematical Assn of Amer, USA.
2. Urrutia J (2000) Art gallery and illumination problems. In: *Handbook of Computational Geometry*, pp 973–1027.
3. Shermer TC (1992) Recent results in art galleries (geometry). *Proc IEEE* **80**, 1384–1399.
4. Ghosh SK (2010) Approximation algorithms for art gallery problems in polygons. *Discret Appl Math*, **158**, 718–722.
5. O'rourke J (1987) *Art Gallery Theorems and Algorithms*, Oxford University Press, UK.
6. Amit Y, Mitchell JS, Packer E (2010) Locating guards for visibility coverage of polygons. *Int J Comput Geom Appl* **20**, 601–630.
7. Eidenbenz S, Stamm C, Widmayer P (2001) Inapproximability results for guarding polygons and terrains. *Algorithmica* **31**, 79–113.

8. Czyzowicz J, Riveracampo E, Urrutia J (1993) Illuminating rectangles and triangles in the plane. *J Comb Theory B* **57**, 1–17.
9. Czyzowicz J, Rivera-Campo E, Urrutia J (1993) Optimal floodlight illumination of stages. In: *Proceedings of the Fifth Canadian Conference on Computational Geometry (CCCG)*, Waterloo, Ontario, Canada, pp 393–398.
10. Jennings SB, Brown ND, Sheil D (1999) Assessing forest canopies and understorey illumination: canopy closure, canopy cover and other measures. *Forestry* **72**, 59–74.
11. Collis RTH (1970) Lidar. *Appl Opt* **9**, 1782–1788.
12. Abegg M, Kükenbrink D, Zell J, Schaepman ME, Morsdorf F (2017) Terrestrial laser scanning for forest inventories—tree diameter distribution and scanner location impact on occlusion. *Forests* **8**, 184.
13. Wilkes P, Lau A, Disney M, Calders K, Burt A, Gonzalez de Tanago J, Brede B (2017) Data acquisition considerations for terrestrial laser scanning of forest plots. *Remote Sens Environ* **196**, 140–153.
14. Kuronen M, Henttonen HM, Myllymäki M (2019) Correcting for nondetection in estimating forest characteristics from single-scan terrestrial laser measurements. *Can J For Res* **49**, 96–103.
15. Li L, Mu X, Soma M, Wan P, Qi J, Hu R (2020) An iterative-mode scan design of terrestrial laser scanning in forests for minimizing occlusion effects. *IEEE Trans Geosci Remote Sens* **59**, 3547–3566.
16. Tóth LF (1977) Illumination of convex discs. *Acta Math Hung* **29**, 355–360.
17. Martini H, Soltan V (1999) Combinatorial problems on the illumination of convex bodies. *Aequationes Math* **57**, 121–152.
18. Berg M, Cheong O, Kreveld M, Overmars M (2008) *Computational Geometry: Algorithms and Applications*, 3rd edn, Springer Berlin, Heidelberg.
19. Devadoss SL, O'Rourke J (2011) *Discrete and Computational Geometry*, Princeton University Press, USA.
20. Boots B, Okabe A, Sugihara K (1999) Spatial tessellations. *Geogr Inf Syst* **1**, 503–526.
21. Aurenhammer F (1987) Power diagrams: properties, algorithms and applications. *SIAM J Comput* **16**, 78–96.
22. Imai H, Iri M, Murota K (1985) Voronoi diagram in the Laguerre geometry and its applications. *SIAM J Comput* **14**, 93–105.
23. Sugihara K (2000) Three-dimensional convex hull as a fruitful source of diagrams. *Theor Comput Sci* **235**, 325–337.

Appendix A. Supplementary data

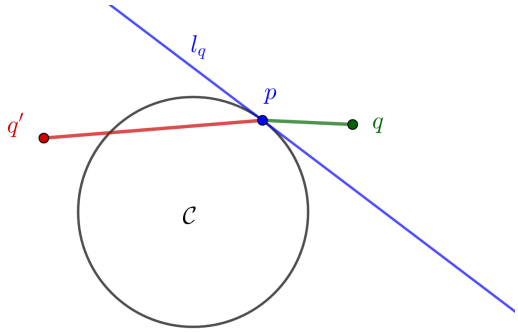

Fig. S1 A point q lying on the side of the half-plane corresponding to the tangent line l_p that does not contain the circular disc C illuminates the point p, whereas a point q' on the opposite side of the half-plane does not.

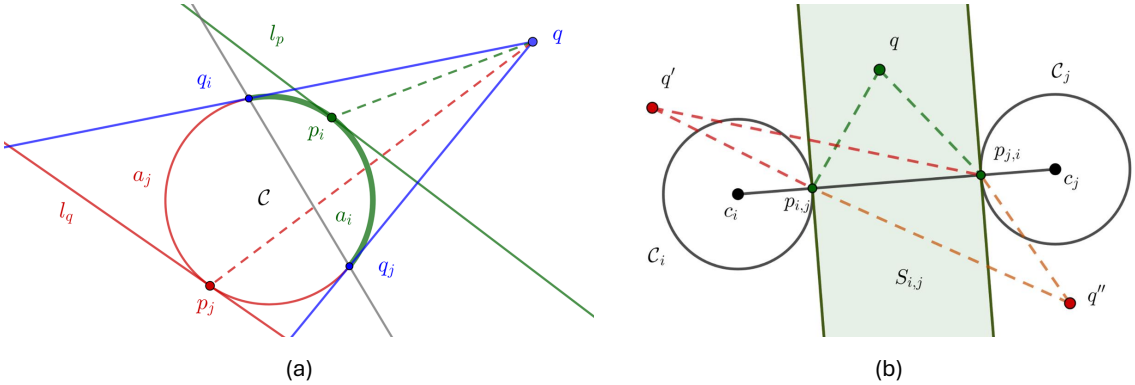

Fig. S2 (a) A point p_i on an arc a_i is visible to q but a point p_j on another arc a_j is not visible. (b) The illuminating point q in a slab $S_{i,j}$ of circular discs C_i and C_j illuminates radial tangent points p_i and p_j, whereas a point q' and q'' outside of $S_{i,j}$ does not.

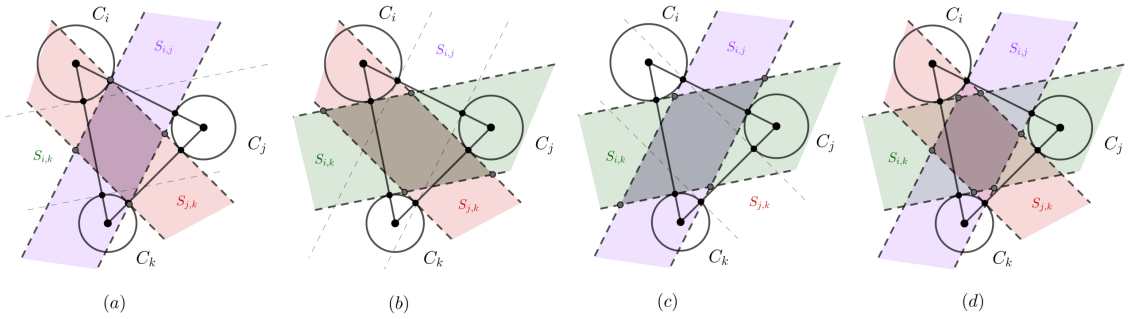

Fig. S3 (a), (b) and (c) show each pair of slabs constructed by three non-overlapping circular discs, forming a parallelogram. (d) Shows the feasible region formed by the intersection of all three slabs.

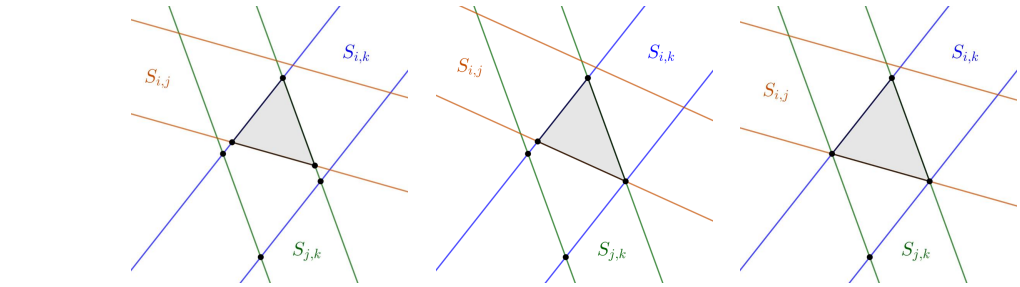

(a)

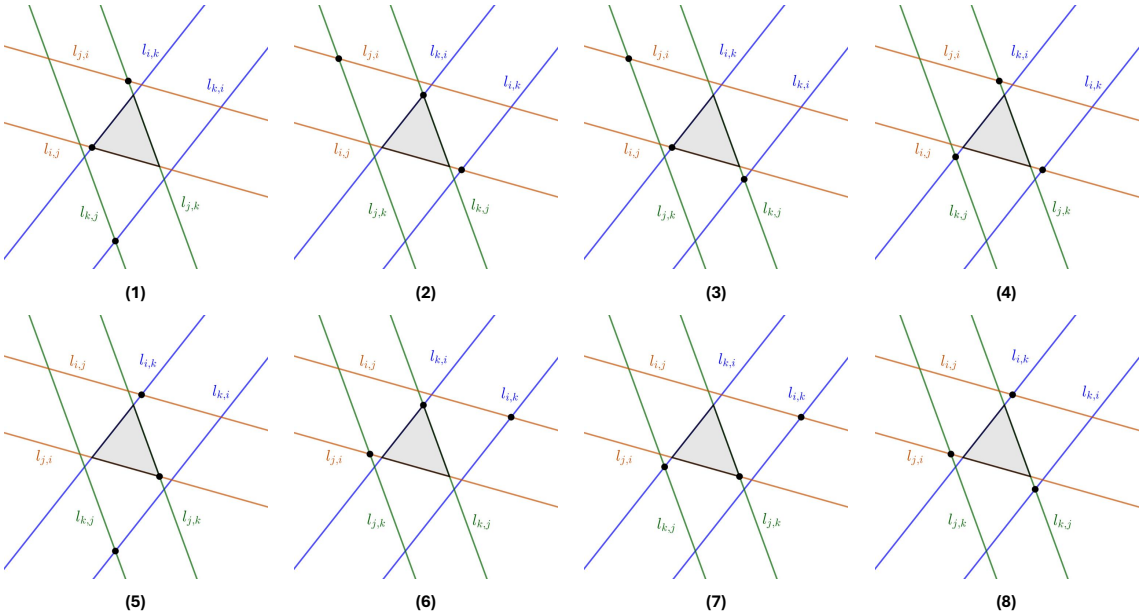

(b)

Fig. S4 (a) Examples of triangular feasible regions: (left) a boundary of $S_{i,j}$ passing through two adjacent edges; (center) a boundary of $S_{i,j}$ passing through one adjacent edge and one adjacent vertex; (right) a boundary of $S_{i,j}$ passing through two adjacent vertices. (b) Examples of triangular feasible region combinations, where combinations (4) and (8) correspond to triangular feasible regions that do not include an intersection point of a pair of tangent lines as a vertex.